



This is a repository copy of *Few-photon all-optical phase rotation in a quantum-well micropillar cavity*.

White Rose Research Online URL for this paper:

<https://eprints.whiterose.ac.uk/194385/>

Version: Accepted Version

---

**Article:**

Kuriakose, T., Walker, P.M. [orcid.org/0000-0002-5431-318X](https://orcid.org/0000-0002-5431-318X), Dowling, T. et al. (13 more authors) (2022) Few-photon all-optical phase rotation in a quantum-well micropillar cavity. *Nature Photonics*, 16 (8). pp. 566-569. ISSN 1749-4885

<https://doi.org/10.1038/s41566-022-01019-6>

---

This version of the article has been accepted for publication, after peer review (when applicable) and is subject to Springer Nature's AM terms of use, but is not the Version of Record and does not reflect post-acceptance improvements, or any corrections. The Version of Record is available online at: <http://dx.doi.org/10.1038/s41566-022-01019-6>

**Reuse**

Items deposited in White Rose Research Online are protected by copyright, with all rights reserved unless indicated otherwise. They may be downloaded and/or printed for private study, or other acts as permitted by national copyright laws. The publisher or other rights holders may allow further reproduction and re-use of the full text version. This is indicated by the licence information on the White Rose Research Online record for the item.

**Takedown**

If you consider content in White Rose Research Online to be in breach of UK law, please notify us by emailing [eprints@whiterose.ac.uk](mailto:eprints@whiterose.ac.uk) including the URL of the record and the reason for the withdrawal request.



[eprints@whiterose.ac.uk](mailto:eprints@whiterose.ac.uk)  
<https://eprints.whiterose.ac.uk/>

# Few-photon all-optical phase rotation in a quantum-well micropillar cavity

Tintu Kuriakose,<sup>1</sup> Paul M. Walker,<sup>1,\*</sup> Toby Dowling,<sup>1</sup> Oleksandr Kyriienko,<sup>2</sup> Ivan A. Shelykh,<sup>3,4</sup> Philippe St-Jean,<sup>5</sup> Nicola Carlon Zambon,<sup>5</sup> Aristide Lemaitre,<sup>5</sup> Isabelle Sagnes,<sup>5</sup> Luc Legratiet,<sup>5</sup> Abdelmounaim Harouri,<sup>5</sup> Sylvain Ravets,<sup>5</sup> Maurice S. Skolnick,<sup>1</sup> Alberto Amo,<sup>6</sup> Jacqueline Bloch,<sup>5</sup> and Dmitry N. Krizhanovskii<sup>1</sup>

<sup>1</sup>*Department of Physics and Astronomy, University of Sheffield, S3 7RH, Sheffield, UK*

<sup>2</sup>*Department of Physics and Astronomy, University of Exeter, EX4 4QL, Exeter, UK*

<sup>3</sup>*Science Institute, University of Iceland, Dunhagi 3, IS-107, Reykjavik, Iceland*

<sup>4</sup>*Department of Physics and Technology, ITMO University, St. Petersburg, 197101, Russia*

<sup>5</sup>*Centre de Nanosciences et de Nanotechnologies (C2N),*

*Université Paris Saclay - CNRS, 911200 Palaiseau, France*

<sup>6</sup>*Univ. Lille, CNRS, UMR 8523 -PhLAM- Physique des Lasers Atomes et Molécules, F-59000 Lille, France*

**Photonic platforms are an excellent setting for quantum technologies because weak photon-environment coupling ensures long coherence times. The second key ingredient for quantum photonics is interactions between photons, which can be provided by optical nonlinearities in the form of cross-phase-modulation (XPM). This approach underpins many proposed applications in quantum optics<sup>1-7</sup> and information processing<sup>8</sup>, but achieving its potential requires strong single-photon-level nonlinear phase shifts and also scalable nonlinear elements. In this work we show that the required nonlinearity can be provided by exciton-polaritons in micropillars with embedded quantum wells. These combine the strong interactions of excitons<sup>9,10</sup> with the scalability of micrometer-sized emitters.<sup>11</sup> We observe XPM up to  $3 \pm 1$  mrad per polariton using laser beams attenuated to below single photon average intensity. With our work serving as a first stepping stone, we lay down a route for quantum information processing in polaritonic lattices.**

Quantum applications of XPM include teleportation<sup>1</sup>, photon-number detection<sup>2</sup>, metrology<sup>4</sup>, cryptography<sup>5</sup>, and quantum information processing (QIP), where it was proposed as a route to circuit-<sup>6</sup> and measurement-<sup>7</sup> based quantum computing. However, XPM-based photonic QIP faces several challenges. Frequency entanglement can degrade the fidelity<sup>12</sup> of XPM-based quantum gates<sup>3</sup>. This can be overcome by cascading nonlinear resonators, with each providing moderate phase shift<sup>8</sup>. Such cascading naturally requires scalability of the resonators. The remaining major challenge, which we address in this paper, is to find a system with high enough single-particle XPM phase shift,  $\phi_{s.p.}$ , which is suitable for scaling.

The small size of atom-like emitters ensures strong interactions and large  $\phi_{s.p.}$  but at the same time makes scalability challenging. Real atoms are not trivial to trap and manipulate while it is difficult to achieve many solid state artificial atoms with deterministic frequencies

and locations. Experimentally,  $\phi_{s.p.}$  from 0.1 to  $\pi$  radians have been observed in atomic ensembles<sup>13-18</sup> and atoms<sup>19</sup> or quantum dots<sup>20,21</sup> strongly coupled to cavities. Methods using electromagnetically induced transparency<sup>16-18</sup> or sequential photon-atom interactions<sup>22,23</sup> achieve  $\phi_{s.p.} = \pi$  using microsecond pulse sequences and milli-Watt ancilliary beams whereas passive-nonlinear XPM, as we study here, is favorable for high rate, low energy operation. Approaches avoiding atom-like emitters have been hindered by the small optical nonlinearity in typical Kerr media.  $\phi_{s.p.}$  from  $10^{-4}$  to 0.3 mrad has been demonstrated with optical fibre<sup>24</sup> and atomic vapours<sup>14,15</sup>. Polariton micropillars, where photons are strongly coupled to excitons,<sup>25</sup> are a prime candidate for combining high phase shifts and scalability. Their micrometer dimensions allow scaling into large lattices with deterministic positioning and energies identical within the linewidth<sup>11</sup>, while the excitonic component of polaritons provides interactions at least 1000 times larger than in weakly coupled and/or bulk semiconductors<sup>26</sup>. An important feature of polariton interactions is their polarization-dependence<sup>27</sup>, which can be used to implement all-optical spin switches<sup>28</sup> or to break time-reversal symmetry. Polaritonic resonators have been utilised as a source of weakly sub-Poissonian light<sup>9,10</sup>. However, neither XPM between distinct modes nor the polarization-dependence of interactions have been harnessed at the few particle level.

In this article we demonstrate  $\phi_{s.p.}$  up to 3 mrad, the highest amount without using atom-like emitters. As a proof of principle we demonstrate this phase rotation using a control laser attenuated down to 0.13 polaritons average intensity, where the probability of  $> 1$  control polariton being in the system is  $< 1\%$ . We exploit the polarisation dependent interactions to encode the XPM on the polarisation state of a second laser, achieving high phase sensitivity and stability. Extrapolating our experimental results to samples with tighter photon confinement and narrower exciton linewidth<sup>9,10</sup>, we predict  $\phi_{s.p.}$  approaching a significant fraction of  $\pi$ . Using the example of XPM-based conditional-phase (CPHASE) quantum gates we show theoretically that these experimental results open new routes towards active quantum processing with exciton polaritons.

---

\* p.m.walker@sheffield.ac.uk

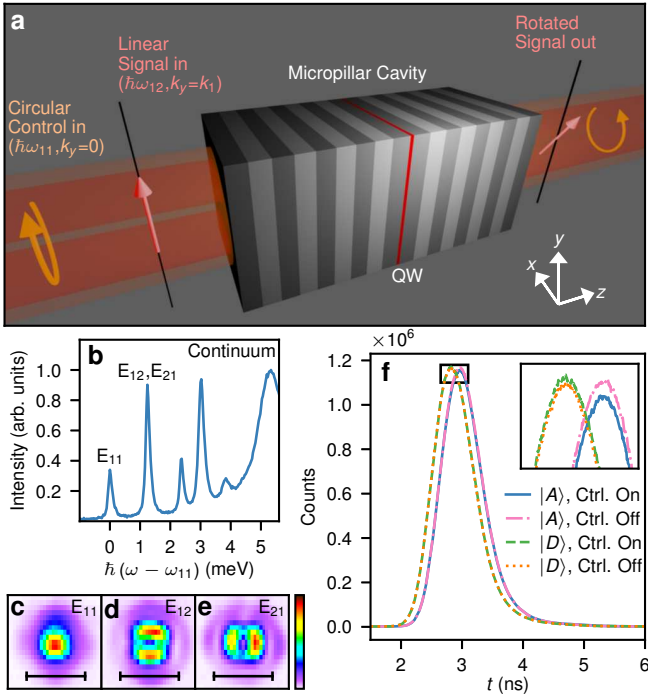


FIG. 1. **Sample properties.** **a**, Schematic of experimental arrangement. **b**, Photoluminescence spectrum from pillar A.  $\hbar\omega_{11} = 1446$  meV. **c-e**, Real space photoluminescence intensity maps taken at the frequencies of the ground ( $E_{11}$ ) and first excited ( $E_{12}$  and  $E_{21}$ ) manifolds. Scale bar corresponds to  $5\ \mu\text{m}$ , which is the size of the micropillar. Colour scale is linear and denotes intensity relative to peak. **f**, Example of raw TCSPC curves recorded during a phase shift measurement.  $|D\rangle$  and  $|A\rangle$  denote the signals from APDs measuring those polarisation components while ‘Ctrl. On’ and ‘Ctrl. Off’ specify the control beam state. The inset to **f** shows a zoom of the region labelled by a black rectangle.

Our device is an AlGaAs air-post Fabry-Perot microcavity containing a single quantum well of the type illustrated in Fig. 1a (see Methods A and Supplementary Discussion 1). All experiments were performed near to liquid helium temperature. We first characterised the micropillar using photoluminescence spectroscopy. The spectrum of discrete states resulting from the three-dimensional optical confinement can be seen in Fig. 1b with mode intensity profiles shown in Fig. 1c-e.

The phase rotation measurement is illustrated in Fig. 1a (see also Supplementary Discussion 1). We resonantly excited  $E_{11}$  with a circularly polarized continuous-wave (CW) beam (control beam) and  $E_{12}$  with a pulsed beam linearly polarised along the  $y$  direction (signal beam). The signal linear polarisation can be decomposed into two circularly polarised components. Since polariton interactions depend strongly on relative circular polarisation<sup>27</sup>, the presence of the control beam shifts the  $E_{12}$  resonance to higher energies only for the polarisation parallel to the control beam. Consequently, the co-polarised signal component acquires a relative phase

shift via XPM, resulting in a rotation of the signal beam linear polarisation angle. Measuring this change in polarisation reveals the amount of phase shift. A quantitative analysis of the XPM and detection process is given in Supplementary Discussion 2. The overall nonlinear phase shift  $\phi$  reads

$$\phi = \frac{2(g_1 - g_2)}{\gamma/2} |X_{11}|^2 |X_{12}|^2 \frac{N_{\text{pol}}}{A_{\text{eff}}}. \quad (1)$$

Here,  $N_{\text{pol}}$  is the mean number of control polaritons present in the cavity,  $A_{\text{eff}}$  is the averaged confinement area of the modes, and  $\gamma$  is the full width at half maximum (FWHM) signal linewidth.  $g_1$  and  $g_2$  are the interaction strengths for co- and cross-circularly-polarised excitons, respectively. The polariton interaction strength increases with the excitonic fractions  $|X_{11}|^2$  and  $|X_{12}|^2$  of the control and signal states. The nonlinear frequency splitting between circular-polarisation states is analogous to a Zeeman splitting caused by an effective magnetic field and the polarisation rotation is analogous to the Faraday effect.

To measure the XPM phase shift we collected the transmitted light, filtered out the control beam using a spectrometer, and measured the diagonal ( $|D\rangle$ ) and anti-diagonal ( $|A\rangle$ ) signal polarisation components with the control beam chopped between on and off. Intensities were measured using time correlated single photon counting (TCSPC) allowing further separation of the pulsed signal beam from the CW control (see Methods D and Supplementary Discussion 3). An example of the TCSPC data is shown in Fig. 1f. The peaks are due to the signal pulses while effects uncorrelated with the signal pulses form a CW background which we measured using points at times far from the peak and subtracted. We then integrated the counts around the peaks to obtain total signal count rates  $I_D^{(\text{on})}$ ,  $I_D^{(\text{off})}$ ,  $I_A^{(\text{on})}$ ,  $I_A^{(\text{off})}$  for the  $|D\rangle$  and  $|A\rangle$ .

Phase shift  $\phi$  is deduced from the difference in polarisation degree with control beam on and off (see Supplementary Discussion 2) and, for small nonlinear resonance shifts compared to the linewidth, is given by

$$\phi \approx \left( \frac{I_D^{(\text{on})} - I_A^{(\text{on})}}{I_D^{(\text{on})} + I_A^{(\text{on})}} \right) - \left( \frac{I_D^{(\text{off})} - I_A^{(\text{off})}}{I_D^{(\text{off})} + I_A^{(\text{off})}} \right). \quad (2)$$

As well as measuring the phase it is important to accurately deduce the number  $N_{\text{pol}}$  of control polaritons in the cavity. The absolute calibration of  $N_{\text{pol}}$  was obtained by measurement of the cavity transfer function, carefully separating the radiative losses from other contributions to the linewidth, which leads to

$$E_{\text{cav}} = \hbar\omega N_{\text{pol}} = \frac{P_{\text{out}}}{\gamma_{\text{T}} |C_{11}|^2} \quad (3)$$

(see Methods E and Supplementary Discussions 4 and 5). Here  $P_{\text{out}}$  is the transmitted power and  $\gamma_{\text{T}}$  is the portion of the bare cavity linewidth associated with

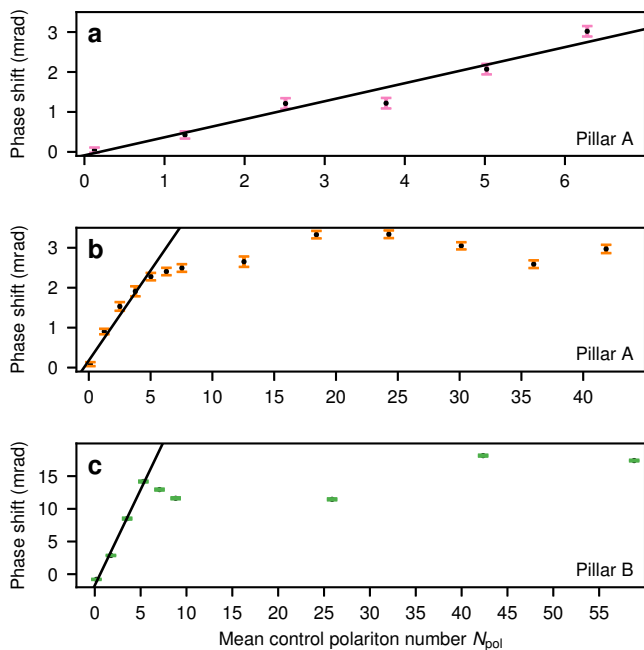


FIG. 2. **Measured phase shift as a function of control beam mean polariton number.** The data in **a** and **b** were measured on pillar A on two different days approximately one month apart. The data in **c** were measured on pillar B. Error bars cover the range  $\pm 2\sigma$  where  $\sigma$  is the standard deviation among the repeated measurements of the phase. The solid lines are best fits of straight lines passing through the origin to points with  $N_{\text{pol}} < 6$ .

transmission through the mirror towards the detector.  $|C_{11}|^2 = 1 - |X_{11}|^2$  is the control polariton photonic fraction. We confirmed the accuracy of Eqn. (3) by exactly solving Maxwell’s equations for a wide range of cavity parameters around those of the experimental device (see Supplementary Discussion 5).

The phase change vs.  $N_{\text{pol}}$  is plotted in Fig. 2. We considered two different micropillar cavities (A and B) with different exciton fractions and linewidths (see Methods A). The phase shift increases with increasing  $N_{\text{pol}}$  between 0.1 and 6 polaritons. Fitting straight lines in this region we deduce slopes of  $0.5 \pm 0.2$  and  $0.5 \pm 0.3$  mrad per polariton for the two pillar A data sets (Fig. 2a and b). For pillar B, which has 7.2x larger  $|X_{11}|^2 |X_{12}|^2$  (see Methods A), the slope was  $3 \pm 1$  mrad per polariton.

Above  $\sim 6$  polaritons (Fig. 2b and c) the phase shift saturates for both pillars. Further experiments are required to identify the mechanism behind this saturation. The dependence on control polarisation is preserved even up to 42 polaritons (Fig. 3a) but with reduced magnitude, suggesting saturation is due to suppression of the polarisation dependence of the effective polariton non-linearity or of the control polariton circular polarisation degree. These can occur due to interaction with a reservoir of excitons, which can be enhanced by sample heating<sup>29–31</sup>. Reservoir accumulation and thermal effects can

be overcome using pulsed, rather than CW, control excitation<sup>26,30</sup>, and by reducing the density of reservoir states using samples with smaller exciton inhomogeneous broadening<sup>32</sup>. We note that saturation will not be detrimental to performance since devices will operate with  $N_{\text{pol}} \leq 1$ .

Inserting our measured slopes for  $\phi(N_{\text{pol}})$  in Eqn. (1) we find they are consistent with  $g_1 - g_2 = 11 \pm 4 \mu\text{eV } \mu\text{m}^2$  and  $10 \pm 4 \mu\text{eV } \mu\text{m}^2$  for pillars A and B respectively. These are at the lower end of the range established by many groups<sup>9,10,26,33–36</sup> indicating that we do not underestimate  $N_{\text{pol}}$ . The agreement between pillars shows that the phase shift scales with exciton fraction as expected. The value 3 mrad per polariton in pillar B is consistent with a blueshift of only  $0.062 \mu\text{eV}$  per polariton compared to the  $E_{12}$  state linewidth  $83 \mu\text{eV}$ , which highlights the sensitivity of the technique.

For our proposed Faraday-like phase rotation mechanism the induced phase should follow a sinusoidal dependence on the angle of the quarter-wave-plate (QWP) used to set the control polarisation, vanishing when the control is linearly polarised and reversing sign when it is switched to the opposite circular polarisation (see Supplementary Discussion 2). In Fig. 3 we show the phase shift vs. the QWP angle for three different control beam strengths covering two orders of magnitude. It agrees well with the theoretical prediction for all control powers, reducing to zero around  $90^\circ$  and then reversing sign. We note that the absolute magnitude of the phase shifts is different to those in Fig. 2 due to day-to-day drifts in sensitivity (see Methods G).

Finally, we discuss the measurements of phase at very low  $N_{\text{pol}} = 0.13 \pm 0.03$ . The data in Figs. 2a and b give phase shifts of  $0.04 \pm 0.06$  and  $0.08 \pm 0.05$  mrad respectively. The four points in Fig. 3c produce phase shifts larger than the uncertainty given by the error bars. We are thus able to measure a phase shift for average powers  $N_{\text{pol}} = 0.13$ , where the probability of the pillar being occupied by a single photon is 11% and the probability of occupancy  $> 1$  is  $< 0.8\%$ , based on the Poissonian statistics expected for laser fields. We are thus well inside the single photon regime.

In Table I we compare the phase shifts available from various systems. Our phase shift of 3 mrad per particle is an order of magnitude larger than in the nearest competing system which does not use atom-like emitters with their associated scalability challenges. Supplementary Discussion 6 provides further detailed comparison. We predict that in samples with tighter photon confinement and narrower exciton linewidth,<sup>9</sup> the phase shift could be two orders of magnitude larger (see Supplementary Discussion 7). Moreover, an additional factor of  $\sim 10$  increase in interactions can also be obtained using dipolar polaritons<sup>37</sup> or trion polaritons<sup>38</sup>.

We measure control (signal) beam transmissions of 45% (35%) in our current devices, limited by a combination of imperfect mode-matching and absorptive losses (see Supplementary Discussion 8 for more de-

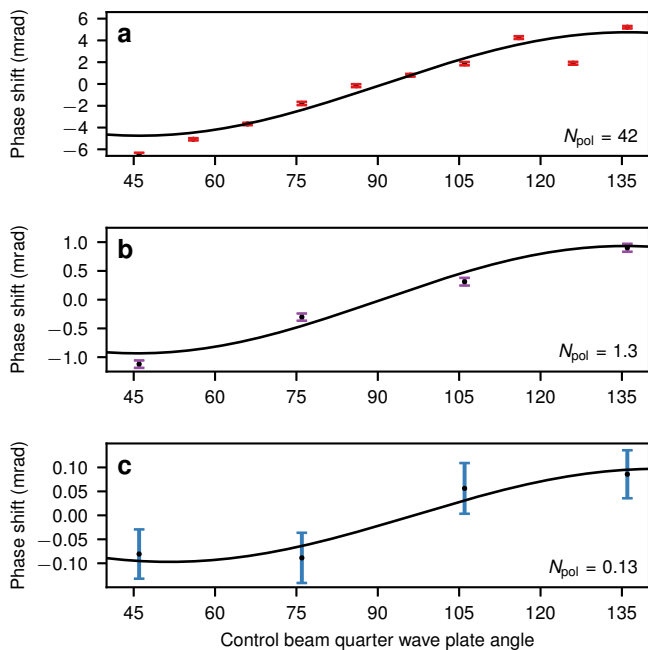


FIG. 3. **Phase shift dependence on control beam polarization.** **a**,  $N_{\text{pol}} = 42 \pm 8$ . **b**,  $N_{\text{pol}} = 1.3 \pm 0.3$ . **c**,  $N_{\text{pol}} = 0.13 \pm 0.03$ . Measurements made on pillar A. Error bars cover the range  $\pm 2\sigma$  where  $\sigma$  is the standard deviation among the repeated measurements of the phase. Solid black lines are best-fit sinusoids.

System	$\phi$ per particle (mrad)
Rydberg atoms in EIT regime <sup>17</sup>	3300
Single Cs Atom <sup>13</sup>	280
Strongly coupled QD <sup>20</sup>	220
<b>This work</b>	<b><math>3 \pm 1</math></b>
Rb vapour in hollow core fibre <sup>14</sup>	0.3
Metastable Xe <sup>15</sup>	0.0003
Photonic crystal fibre <sup>24</sup>	0.0001

TABLE I. Comparison of XPM phase shift platforms.

tails). Transmission can realistically be increased above 90% using lower temperature  $\sim 4$  K and GaAs quantum wells, which have lower inhomogeneous broadening<sup>32</sup>. This would allow transmission through multiple pillars with a  $1/e$  decay of  $\sim 10$  sites. The signal transmission is independent of control polarisation and has a weak dependence on control power arising from blueshift of the states relative to resonance with the signal laser (Methods E). To maximise transmission, low sample temperatures of 4 K (easily achieved using commercial closed cycle cryostats) are important, in comparison to Refs. 14, 15, 18, and 24 where room temperature phase shifts were demonstrated.

Having demonstrated XPM for single-polariton intensities it is interesting to consider whether XPM-based effects can be used for polaritonic QIP. Entanglement be-

tween frequency states was shown to limit the fidelity of XPM-based CPHASE gates for large phase shifts<sup>12</sup>. This obstacle can be overcome if nonlinearity is distributed over several cavities with cascaded wavepacket propagation<sup>8</sup>. In Supplementary Discussion 9 we analyse theoretically a potential scheme to achieve this. It requires scattering through order 10 resonators and optical circulation (suppressed backscattering). Micropillar lattices of this scale are regularly produced while directional propagation from one phase-shift element to the next can be achieved using the edge states in polariton topological insulator lattices and benefit from the rich topological physics of polaritons<sup>39</sup>.

As we show in Supplementary Fig. 10 CPHASE gate fidelity depends on the size of the single-pillar phase shifts and the target phase. Full  $\pi$  shift, corresponding to high-fidelity controlled-Z gate, requires large single-pillar nonlinearity-to-linewidth ratio  $U_{\text{pp}}/\gamma$ . However even with  $U_{\text{pp}}/\gamma < 1$  near perfect fidelity  $\pi/m$  gates (integer  $m$ ) can be achieved. When concatenated these contribute to a universal gateset and, for  $m = 6$ , have been used in quantum hardware-based solution of optimization problems<sup>40</sup>.

While being a distant goal, we consider the ability to inject nonlinearity at the single polariton level a crucial element for many QIP protocols. In general terms, our QW polariton approach to single photon phase shifts provides the tools to optimise the balance between scalability and interaction strength for any given application. In summary, we demonstrated a few-particle polariton XPM phase shift in a scalable on-chip platform. This opens up new approaches to a wide class of nonlinear quantum optical phenomena, and offers a route towards QIP with polaritonic lattices.

## METHODS AND MATERIALS

### A. Sample properties

The sample consists of a GaAs cavity containing a single 15nm wide  $\text{In}_{0.05}\text{Ga}_{0.95}\text{As}$  QW at the electric field antinode and embedded between two  $\text{Al}_{0.1}\text{Ga}_{0.9}\text{As}/\text{Al}_{0.95}\text{Ga}_{0.05}\text{As}$  Bragg mirrors. Confinement of the light in all three dimensions results in discrete optical modes, which were measured using imaging PL spectroscopy (Fig. 1 b-e). The transverse mode profiles are similar to Hermite-Gauss modes. In the ground state manifold, labelled  $E_{11}$ , there are two degenerate polarisation states. In the first excited manifold the sub-manifolds  $E_{12}$  and  $E_{21}$ , have non-zero wavevector component in the  $y$  and  $x$  direction respectively and each contains two orthogonal polarisation states. There is a small splitting among these four states due to a combination of TE-TM splitting and the pillars not being perfectly square. The splitting between the  $E_{21}$  and  $E_{12}$  sub-manifolds allowed them to be mapped separately (Fig. 1d,e) using energies one FWHM either side of the

peak (see methods C).

The studied sample contains many pillars with different sizes (width from  $2\ \mu\text{m}$  to  $5\ \mu\text{m}$ ) to allow tuning of the spatial distribution of modes and their energy separation. The spacing between individual pillars was  $10\ \mu\text{m}$ . Different detunings of pillar modes with respect to the QW exciton resonance were also available due to a wedge in the MBE-grown cavity. The experiments presented in this paper were performed on  $5\ \mu\text{m} \times 5\ \mu\text{m}$  square pillars. The square geometry allowed simple excitation of the Hermite-Gauss-like first excited state compared to more difficult beam shaping required to excite the Laguerre-Gauss-like excited states of a circular pillar. The  $5\ \mu\text{m}$  size of the pillars minimised TE-TM splitting of the first excited manifold.

The sample Rabi splitting  $3.4 \pm 0.1\ \text{meV}$  was obtained from a coupled exciton-photon oscillator model fit to the dispersion of pillar modes. To determine the detuning of the modes from the exciton we compared the energy splitting between the  $E_{11}$  and  $E_{12}$  modes with the value for very negatively detuned pillars. The splitting reduces as the photonic fraction reduces and so can be used to directly obtain the photonic (and hence excitonic) fraction of the polaritons. For pillar A the exciton fractions in the control and signal modes were  $|X_{11}|^2 \sim 9\%$  and  $|X_{12}|^2 \sim 15\%$  respectively. For pillar B they were  $|X_{11}|^2 \sim 25\%$  and  $|X_{12}|^2 \sim 42\%$ .

The polariton linewidths ( $90\ \mu\text{eV}$  and  $83\ \mu\text{eV}$  for pillars A and B respectively) were measured by monitoring the transmitted intensity of a single mode laser as it was scanned through the modes. The measured linewidths are considerably larger than the planar cavity linewidths predicted by transfer matrix method ( $20\text{-}30\ \mu\text{eV}$ ), which is most likely due to absorptive losses associated with elevated sample temperature. In sample-in-vacuum cold-finger cryostats of the type we used sample temperatures are typically higher ( $\sim 10\text{-}20\ \text{K}$ ) than the  $4\ \text{K}$  temperature measured at the heat-exchanger owing to radiation through cryostat optical windows and limited thermal conductivity between the sample and the liquid helium loop. In other types of cryostat, such as sample-in-vapour type, lower temperatures  $\sim 4\ \text{K}$  can be achieved. We note that for deducing the number of polaritons we use the fraction of the linewidth due to radiative transmission towards the detector,  $\gamma_T = 14 \pm 3\ \mu\text{eV}$  in Eqn. (3) (see methods E). This was calibrated at detunings far from the exciton, where absorption is negligible.

The effective mode area for nonlinear interactions  $A_{\text{eff}}$  is defined in Supplementary Discussion 2 following the standard formula from nonlinear fiber-optics. It has the same value  $A_{\text{eff}} = 17\ \mu\text{m}^2$  for both pillars. It was calculated using the modes of a square dielectric rod of GaAs in air obtained from the commercial eigenmode solver Lumerical MODE.

## B. Common experimental details

Experiments were performed near to liquid helium temperature. The sample was held in vacuum and mounted to a copper block connected to the heat-exchanger of a continuous flow cryostat. The copper block was held at less than  $5\ \text{Kelvin}$ , as measured using a silicon diode temperature sensor. Radiation load through the cryostat windows and the small transverse area for heat flow in a  $5\ \mu\text{m}$  square micropillar may have caused the actual pillar temperatures to be higher.

The micropillars were optically excited directly (not through the substrate) using a  $4\ \text{mm}$  focal length objective (numerical aperture 0.42). Light emitted by or transmitted through the pillars was collected by a  $10\ \text{mm}$  focal length microscope objective (numerical aperture 0.6) and imaged via a set of confocal lenses onto the entrance slit of an imaging spectrometer. The spectrometer output could be switched between a CCD camera and an exit slit used to select only the signal beam for the APD measurements. The spectrometer exit slit was imaged onto the APDs via another pair of confocal lenses.

## C. Photoluminescence experiments

For the non-resonant photo-luminescence (PL) experiments excitation was with a laser at  $\sim 830\ \text{nm}$ , above the quantum well band edge, and all optical states were then populated by hot carrier relaxation. The PL spectra were recorded using a CCD camera. Mode intensity profiles were obtained by scanning the images of the modes across the spectrometer entrance slit.  $E_{12}$  and  $E_{21}$  were mapped separately using frequencies one FWHM ( $70\text{-}90\ \mu\text{eV}$ ) either side of the peak. This relies on a small energy splitting between  $E_{12}$  and  $E_{21}$  most likely caused by slightly non-square pillars. As can be seen in Fig. 1b the splitting was too small to resolve directly from the spectrum.

## D. Phase rotation measurement details

For the phase rotation experiments we resonantly excited the micropillar ground state with a circularly polarized control beam emitted by a CW single mode laser. At the same time, we also excited the  $E_{12}$  pillar mode with a linearly polarized signal beam from a tuneable mode-locked Ti:Sapphire laser with a pulse duration of  $\sim 100\ \text{ps}$  and a repetition rate of  $80\ \text{MHz}$ . The sizes and divergences of the input control and signal beams were controlled with telescopes to match those of the pillar modes and hence optimally couple light to the microcavity. Both the signal and control beam were set to have a flat-phase beam waist of  $\sim 3\ \mu\text{m}$  (FWHM) on the sample surface, matching the ground mode FWHM. After this, a phase mask was placed at the focus of the telescope controlling the signal beam in order to introduce a

$\pi$  phase jump at the center of the signal spot on the sample surface. In this way the signal beam was converted to a Hermite-Gauss-like beam with symmetry matching that of the  $E_{12}$  mode but of the wrong symmetry to excite the  $E_{21}$  mode. To ensure that experimental drifts did not compromise optimal coupling the transmission of the control and signal beams was checked after every data point shown in Figs. 2 and 3 and re-optimized if necessary.

Measurement of the intensities of the two polarisation components was performed by photon counting using avalanche photodiodes (APDs) owing to their extremely small noise level. The control beam was chopped on and off at a rate of 10kHz using an electro-optic modulator driven by a square wave control signal. Counts from the APDs were sent to a time-correlated single photon counting card (TCSPC) via a router which encoded information about which APD detected the photon and whether the chopped control beam was on or off. The signal beam was attenuated so that typically 0.025 photons were detected per laser pulse on average. We avoided spurious signals in several ways. Since the control beam was CW while the signal was pulsed (see Fig. 1f) we were able to remove any potential scattered control light reaching the APDs by subtracting the CW background from the data. This also removed any dark or APD after-pulsing counts. The true signal counts were then obtained by summing counts around the signal peaks in the TCSPC traces. Since we measure a polarisation degree of the form shown in Eqn. (2) any overall drifts or jitter in signal beam intensity or integration time simply cancel out. Our chopping of the control beam at 10 kHz eliminates any control drift effects in a manner similar to lock-in detection, while collection over several minutes effectively averages out control beam jitter. Further details are given in Supplementary Discussion 3.

### E. Number of polaritons

The number of control polaritons in the pillar  $N_{\text{pol}}$  was deduced using the transmitted power and the radiative loss rate through the mirror on the transmission side of the sample,  $\gamma_{\text{T}}$ . The accuracy of Eqn. 3 was confirmed by comparison of transmitted power and stored electromagnetic energy using exact solutions of Maxwell's equations (transfer matrix method) for cavities with a wide range of parameters around those of the experimental device (see Supplementary Discussion 5 for a detailed discussion).

The total radiative loss through both mirrors was obtained by measuring the linewidth  $\gamma_{\text{DBR}} = 25 \pm 5 \mu\text{eV}$  at a very photonic detuning where the losses are dominated by the finite reflectivity of the mirrors. It agrees well with transfer matrix simulations. We then use  $\gamma_{\text{T}} = \eta \cdot \gamma_{\text{DBR}}$  where  $\eta = 0.553$  is related to the relative mirror strengths and was obtained from the transfer matrix simulations.

In principle either the incident or transmitted power can be used to obtain  $N_{\text{pol}}$ . We obtain a high transmis-

sion through the pillar with transmitted/incident power being 40% (45%) for the control state of pillar A (B). It is more accurate to use the transmitted power since incident power can be reflected due to imperfect mode matching.

The signal state transmission was 35% for the best coupling to the pillars that we achieved. The laser pulses incident on the pillar contained 27 photons on average. The transmitted pulses contained between 3 and 9 photons depending on coupling, corresponding to peak internal number of polaritons between 2 and 5 for pillar A and 3 and 8 for pillar B. We did not observe any dependence of the results on the number of signal polaritons.

The dependence of total signal beam transmission on the control was obtained by adding the intensities of both APDs (See Supplementary Discussion 8). We found no systematic dependence of the signal transmission on control beam polarisation. The signal transmission vs. control power varied with gradient similar in magnitude to the phase shift and with either positive or negative sign depending on the data set. This is consistent with a blueshift of the states shifting them further into or out of resonance with the signal laser (see Supplementary Discussion 2).

### F. Statistical analysis

By calculating the mean and standard deviation  $\sigma$  among many ( $10^3$ - $10^4$ ) repeated measurements of  $\phi$ , we directly obtain the average phase change and its uncertainty for each value of  $N_{\text{pol}}$  or quarter wave plate angle. The quoted uncertainties are  $\pm 2\sigma$  and the error bars are plotted covering the range from  $-2\sigma$  to  $+2\sigma$ , which corresponds to the 95% confidence interval for a normal distribution.

### G. Sources of noise in the data

There are two categories of noise contributing to the data shown in Figs. 2 and 3. These are a random error in the phase of each individual data point, and systematic variations in sensitivity which occurred between individual data points and different data sets (see supplementary discussion 3). The former arises from the Poissonian counting statistics. The latter arises because sublinewidth changes in signal beam detuning can change the sensitivity of the measurement to the blueshift of the states. The small changes in detuning were caused by slow frequency drift during data collection, necessitating slight re-tuning between data points, and also by the coarse tuning (limited to  $\sim 20 - 30 \mu\text{eV}$  accuracy) of our 100 ps pulsed laser. The sensitivity function is Lorentzian with the state linewidth (see Supplementary Discussion 2). During data collection small experimental drifts were corrected in-between recording each data point, resulting in small changes in sensitivity and hence some point-to-

point noise. Nevertheless, the overall trends are clearly visible in the curves presented in Figs. 2 and 3 and they agree well with theory so we can be confident that this point-to-point noise is not too large. The dependence of sensitivity on small changes in signal laser detuning also causes small differences in scaling from one data set to another, hence the best-fit peak phase shift for  $N_{\text{pol}} = 42$  polaritons in Fig. 3a is  $5 \pm 1$  mrad, slightly larger than the maximum value in Fig. 2b ( $3.3 \pm 0.1$ ), which was measured on a different day.

#### DATA AVAILABILITY

The data supporting the findings of this study are freely available in the University of Sheffield repository with the identifier [doi:10.15131/shef.data.14744121](https://doi.org/10.15131/shef.data.14744121).

#### CODE AVAILABILITY

The custom codes used in this study are available from the corresponding author upon reasonable request.

#### ACKNOWLEDGEMENTS

This work was supported by the Engineering and Physical Sciences Research Council grants EP/N031776/1 and EP/V026496/1, the QUANTERA project Interpol (EP/R04385X/1 and ANR-QUAN-0003-05), the Paris Ile-de-France Région in the framework of DIM SIRTEQ, ERC StG ARQADIA (949730) and CoG EMERGEN-

TOPO (865151), the Marie Skłodowska-Curie individual fellowship ToPol, the H2020-FETFLAG project PhoQus (820392) and the French RENATECH network. O. K. acknowledges the support from UK EPSRC New Investigator Award (EP/V00171X/1). A. A. acknowledges support from the Labex CEMPI (ANR-11-LABX-0007). I. A. S. acknowledges support from IRF (project ‘‘Hybrid polaritonics’’) and Priority 2030 Federal Academic Leadership Program.

#### AUTHOR CONTRIBUTIONS

P. M. W. and D. N. K. conceived and designed the experiment. T. K., P. M. W. and T. D. built the experimental apparatus and performed the experiments. P. S.-J., N. C.Z., A. A., S. R. and J. B. designed and characterized the sample. A.L, IS, L.L and A.H fabricated the sample. P. M. W. analysed the data and wrote the manuscript and supplementary material with contributions from T. K. and O. K. O. K. developed the quantum theoretical description of XPM CPHASE gates. P.M.W. developed the classical theory for cavity occupancy and XPM polariton polarisation rotation. All authors contributed to discussion of the data and discussion and revision of the manuscript.

#### COMPETING INTERESTS

The authors declare that there are no competing interests.

- 
- <sup>1</sup> Vitali, D., Fortunato, M. & Tombesi, P. [Complete quantum teleportation with a kerr nonlinearity](#). *Physical Review Letters* **85**, 445–448 (2000).
  - <sup>2</sup> Munro, W. J., Nemoto, K., Beausoleil, R. G. & Spiller, T. P. [High-efficiency quantum-nondemolition single-photon-number-resolving detector](#). *Physical Review A* **71**, 033819 (2005).
  - <sup>3</sup> Spiller, T. P. *et al.* [Quantum computation by communication](#). *New Journal of Physics* **8**, 30–30 (2006).
  - <sup>4</sup> Joo, J., Munro, W. J. & Spiller, T. P. [Quantum metrology with entangled coherent states](#). *Physical Review Letters* **107**, 083601 (2011).
  - <sup>5</sup> Simon, D. S., Jaeger, G. & Sergienko, A. V. [Entangled-coherent-state quantum key distribution with entanglement witnessing](#). *Physical Review A* **89**, 012315 (2014).
  - <sup>6</sup> Chuang, I. L. & Yamamoto, Y. [Simple quantum computer](#). *Physical Review A* **52**, 3489–3496 (1995).
  - <sup>7</sup> Hutchinson, G. D. & Milburn, G. J. [Nonlinear quantum optical computing via measurement](#). *Journal of Modern Optics* **51**, 1211–1222 (2004).
  - <sup>8</sup> Brod, D. J., Combes, J. & Gea-Banacloche, J. [Two photons co- and counterpropagating through  \$N\$  cross-Kerr sites](#). *Physical Review A* **94**, 023833 (2016).
  - <sup>9</sup> Delteil, A. *et al.* [Towards polariton blockade of confined exciton–polaritons](#). *Nature Materials* **18**, 219–222 (2019).
  - <sup>10</sup> Muñoz-Matutano, G. *et al.* [Emergence of quantum correlations from interacting fibre-cavity polaritons](#). *Nature Materials* **18**, 213–218 (2019).
  - <sup>11</sup> Amo, A. & Bloch, J. [Exciton-polaritons in lattices: A nonlinear photonic simulator](#). *Comptes Rendus Physique* **17**, 934–945 (2016).
  - <sup>12</sup> Shapiro, J. H. [Single-photon kerr nonlinearities do not help quantum computation](#). *Physical Review A* **73**, 062305 (2006).
  - <sup>13</sup> Turchette, Q. A., Hood, C. J., Lange, W., Mabuchi, H. & Kimble, H. J. [Measurement of conditional phase shifts for quantum logic](#). *Physical Review Letters* **75**, 4710–4713 (1995).
  - <sup>14</sup> Venkataraman, V., Saha, K. & Gaeta, A. L. [Phase modulation at the few-photon level for weak-nonlinearity-based quantum computing](#). *Nature Photonics* **7**, 138–141 (2012).
  - <sup>15</sup> Hickman, G. T., Pittman, T. B. & Franson, J. D. [Low-power cross-phase modulation in a metastable xenon-filled cavity for quantum-information applications](#). *Physical Review A* **92**, 053808 (2015).

- <sup>16</sup> Liu, Z.-Y. *et al.* Large cross-phase modulations at the few-photon level. *Physical Review Letters* **117**, 203601 (2016).
- <sup>17</sup> Tiarks, D., Schmidt, S., Rempe, G. & Dürr, S. Optical  $\pi$  phase shift created with a single-photon pulse. *Science Advances* **2**, e1600036 (2016).
- <sup>18</sup> Sagona-Stophel, S., Shahrokshahi, R., Jordaan, B., Namazi, M. & Figueroa, E. Conditional  $\pi$ -phase shift of single-photon-level pulses at room temperature. *Phys. Rev. Lett.* **125**, 243601 (2020).
- <sup>19</sup> Volz, J., Scheucher, M., Junge, C. & Rauschenbeutel, A. Nonlinear  $\pi$  phase shift for single fibre-guided photons interacting with a single resonator-enhanced atom. *Nature Photonics* **8**, 965–970 (2014).
- <sup>20</sup> Fushman, I. *et al.* Controlled phase shifts with a single quantum dot. *Science* **320**, 769–772 (2008).
- <sup>21</sup> Englund, D. *et al.* Ultrafast photon-photon interaction in a strongly coupled quantum dot-cavity system. *Physical Review Letters* **108**, 093604 (2012).
- <sup>22</sup> Hacker, B., Welte, S., Rempe, G. & Ritter, S. A photon-photon quantum gate based on a single atom in an optical resonator. *Nature* **536**, 193–196 (2016).
- <sup>23</sup> Sun, S., Kim, H., Luo, Z., Solomon, G. S. & Waks, E. A single-photon switch and transistor enabled by a solid-state quantum memory. *Science* **361**, 57–60 (2018).
- <sup>24</sup> Matsuda, N., Shimizu, R., Mitsumori, Y., Kosaka, H. & Edamatsu, K. Observation of optical-fibre kerr nonlinearity at the single-photon level. *Nature Photonics* **3**, 95–98 (2009).
- <sup>25</sup> Bajoni, D. *et al.* Polariton laser using single micropillar GaAs-GaAlAs semiconductor cavities. *Physical Review Letters* **100**, 047401 (2008).
- <sup>26</sup> Walker, P. M. *et al.* Dark solitons in high velocity waveguide polariton fluids. *Phys. Rev. Lett.* **119**, 097403 (2017).
- <sup>27</sup> Vladimirova, M. *et al.* Polariton-polariton interaction constants in microcavities. *Physical Review B* **82**, 075301 (2010).
- <sup>28</sup> Amo, A. *et al.* Exciton-polariton spin switches. *Nature Photonics* **4**, 361–366 (2010).
- <sup>29</sup> Vishnevsky, D. V., Solnyshkov, D. D., Gippius, N. A. & Malpuech, G. Multistability of cavity exciton polaritons affected by the thermally generated exciton reservoir. *Phys. Rev. B* **85**, 155328 (2012).
- <sup>30</sup> Sekretenko, A. V., Gavrilov, S. S. & Kulakovskii, V. D. Polariton-polariton interactions in microcavities under a resonant 10 to 100 picosecond pulse excitation. *Phys. Rev. B* **88**, 195302 (2013).
- <sup>31</sup> Ouellet-Plamondon, C. *et al.* Reservoir-induced decoherence of resonantly excited confined polaritons. *Phys. Rev. B* **95**, 085302 (2017).
- <sup>32</sup> Borri, P., Langbein, W., Woggon, U., Jensen, J. R. & Hvam, J. M. Microcavity polariton linewidths in the weak-disorder regime. *Physical Review B* **63**, 035307 (2000).
- <sup>33</sup> Amo, A. *et al.* Superfluidity of polaritons in semiconductor microcavities. *Nature Physics* **5**, 805–810 (2009).
- <sup>34</sup> Vladimirova, M. *et al.* Polarization controlled nonlinear transmission of light through semiconductor microcavities. *Physical Review B* **79**, 115325 (2009).
- <sup>35</sup> Brichkin, A. S. *et al.* Effect of Coulomb interaction on exciton-polariton condensates in GaAs pillar microcavities. *Phys. Rev. B* **84**, 195301 (2011).
- <sup>36</sup> Estrecho, E. *et al.* Direct measurement of polariton-polariton interaction strength in the thomas-fermi regime of exciton-polariton condensation. *Physical Review B* **100**, 035306 (2019).
- <sup>37</sup> Rosenberg, I. *et al.* Strongly interacting dipolar-polaritons. *Science Advances* **4**, eaat8880 (2018).
- <sup>38</sup> Emmanuele, R. P. A. *et al.* Highly nonlinear trion-polaritons in a monolayer semiconductor. *Nature Communications* **11**, 3589 (2020).
- <sup>39</sup> Solnyshkov, D. D. *et al.* Microcavity polaritons for topological photonics [invited]. *Optical Materials Express* **11**, 1119 (2021).
- <sup>40</sup> Harrigan, M. P. *et al.* Quantum approximate optimization of non-planar graph problems on a planar superconducting processor. *Nature Physics* **17**, 332 (2021).